

Diffusivity dependence of the transition path ensemble

Lukas Kikuchi,* Ronojoy Adhikari, and Julian Kappler
 DAMTP, Centre for Mathematical Sciences, University of Cambridge,
 Wilberforce Road, Cambridge CB3 0WA, UK

At low temperatures transition pathways of stochastic dynamical systems are typically approximated by instantons. Here we show, using a dynamical system containing two competing pathways, that even at low-to-intermediate temperatures, instantons can fail to capture the most likely transition pathway. We consider an approximation which includes Gaussian fluctuations around instantons and, by comparing with the results of an accurate and efficient path-space Monte Carlo sampling method, find this approximation to hold for a wide range of temperatures. Our work delimits the applicability of large deviation theory and provides methods to probe these limits numerically.

The fluctuating dynamics of many physical, chemical and biological systems are commonly modelled by stochastic differential equations expressed in Langevin or Itô forms [1–4]. In such systems it is often of great interest to identify the typical pathways that stochastic paths take to transition from an initial to a final state, as for example in the nucleation of solids, the conformational changes in biomolecules, or shifts in ecological balance [5–13]. Typically, such transition paths cluster around multiple pathways in the space of configurations and the relative probability of one or the other of these pathways depends on the drift, the diffusivity, and the duration allowed for the transition to take place [14–17]. As transitions are often rare events, direct simulations are not always practical and other means, analytical or numerical, are required to study them. Methods that allow for a full exploration of the space of transition pathways in stochastic dynamical systems, then, are of substantial theoretical and practical importance.

The theory of large deviations [18–21] provides an analytical method for obtaining transition pathways - instantons - in regimes dominated by the drift and for very long durations of path. Experimental systems, however, are typically not in a regime where the diffusivity is asymptotically low and durations are asymptotically long [75]. While the relevance of including finite-temperature fluctuations around the instanton [68] is increasingly recognized [24–26], the physical implications of these fluctuations are far from being understood.

In this Letter, we show that the competition between drift and diffusion in transition pathways can be studied using semi-classical expansions of the path measure of the stochastic dynamics. We use a mixture of Gaussian measures to approximate the path measure around its local instantons. This allows us to demarcate and transcend the boundaries of the low diffusivity regime. We demonstrate this explicitly for a two-dimensional overdamped me-

chanical system, with both conservative and non-conservative forces. For this system we uncover a counterintuitive phenomenon where typical transition paths do not concentrate around the most probable path, even at low-to-intermediate diffusivities where the Gaussian approximation is still valid. To validate our results numerically, we construct a Markov Chain Monte Carlo (MCMC) method that allows for simultaneous exploration of multiple transition pathways. We find excellent agreement between the semi-classical expansion and numerical results for a large range of diffusivities and path durations. We now detail our results.

The transition path ensemble. We consider the stochastic process generated by the d -dimensional overdamped Langevin equation, expressed in Itô form as

$$d\mathbf{X} = \mu\mathbf{F}dt + \sqrt{2D}d\mathbf{W}. \quad (1)$$

This represents the stochastic displacement $d\mathbf{X}$ in a time interval dt of a particle with coordinate \mathbf{X} subject to a force field \mathbf{F} and Brownian displacements $\sigma d\mathbf{W}$, where \mathbf{W} is the Wiener process. The particle mobility is μ , the diffusion constant is $D = \mu/\beta$, and the temperature is θ with $\beta^{-1} = k_B\theta$, and k_B the Boltzmann constant. We are interested in realisations $\mathbf{X}(t)$ of Eq. (1) that are of duration T and have fixed termini $\mathbf{X}(0) = \mathbf{x}_0$ and $\mathbf{X}(T) = \mathbf{x}_T$. These trajectories form a set of continuous paths that we call the transition path ensemble (TPE). While in the following we investigate the temperature-dependence of the TPE for specific model systems, the methods we develop are general.

Model system. We consider the motion of a particle in $d = 2$ dimensions in a potential force field $\mathbf{F} = -\nabla U(\mathbf{x})$; below we will also add a non-conservative force \mathbf{F}^a . The potential $U(\mathbf{x})$ is a deformed Mexican hat, with a maximum at the origin and a manifold of minima on the circle of radius L around the origin,

see Fig. 1 (a) for a plot of U and the SI for the explicit parametrisation [27]. We consider the TPE for paths of duration T which start at $\mathbf{x}_0 = (-L, 0)$ and end at $\mathbf{x}_T = (L, 0)$. This ensemble features two competing transition channels, namely along the upper and lower semi-circle, which we denote by Γ^+ and Γ^- ; by design the potential along Γ^+ is narrower as compared to along Γ^- .

Gaussian mixture approximation of the TPE. The TPE is characterized by its corresponding probability measure \mathbb{P} on the space of all continuous transition paths. In the path-integral formalism, this measure is represented by a formal density $\rho[\mathbf{x}(t)] = \exp(-S_{\text{OM}}[\mathbf{x}(t)])$ with respect to a fictitious infinite-dimensional Lebesgue measure [72], with the Onsager-Machlup action [14–16]

$$S_{\text{OM}}[\mathbf{x}(t)] = \int_0^T \left(\frac{\beta}{4\mu} |\dot{\mathbf{x}} - \mathbf{F}|^2 + \frac{\mu}{2} \nabla \cdot \mathbf{F} \right) dt. \quad (2)$$

The variational minima of the action Eq. (B5) have physical relevance. Namely, because the first term in Eq. (B5) is inversely proportional to the temperature, at sufficiently low temperature the formal probability density ρ is dominated by paths that aggregate around the variational minima [18–20]. These variational minima are called the local instantons of the Onsager-Machlup action, and we denote them by $\mathbf{x}^{[\alpha]}(t; \theta, T)$, with $\alpha = 1, \dots, K$, $\mathbf{x}^{[\alpha]}(0; \theta, T) = \mathbf{x}_0$ and $\mathbf{x}^{[\alpha]}(T; \theta, T) = \mathbf{x}_T$. The arguments of the local instantons indicate that they depend on the temperature and the duration of the path (we suppress these arguments below). For the potential U from Fig. 1 (a) we find $K = 2$ local instantons $\mathbf{x}^{[1]} \equiv \mathbf{x}^+$, $\mathbf{x}^{[2]} \equiv \mathbf{x}^-$, going along the upper and lower semi-circles, respectively.

By performing a quadratic functional Taylor expansion of Eq. (B5) around the α -th local instanton [29–31],

$$S_{\text{OM}}[\mathbf{x}(t)] \approx S_{\text{OM}}[\mathbf{x}^{[\alpha]}(t)] + \frac{1}{2} \langle \delta \mathbf{x}, \mathcal{H}^{[\alpha]} \delta \mathbf{x} \rangle, \quad (3)$$

where $\mathcal{H}^{[\alpha]}$ is a self-adjoint linear differential operator, $\delta \mathbf{x} = \mathbf{x} - \mathbf{x}^{[\alpha]}$ and $\langle \mathbf{f}, \mathbf{g} \rangle = \sum_i \int_0^T f_i(t) g_i(t) dt$, we can formally define a Gaussian measure $\mathbb{P}^{[\alpha]}$ with mean $\mathbf{x}^{[\alpha]}$, precision $\mathcal{H}^{[\alpha]}$, and regularised normalisation constant $\mathcal{Z}^{[\alpha]}$, in the space of paths. The resulting K local approximators of the measure can be combined into a Gaussian mixture approximation [67] of the whole TPE

$$\mathbb{P} \approx \bar{\mathbb{P}} \equiv \sum_{\alpha=1}^K w_{\alpha} \mathbb{P}^{[\alpha]}, \quad (4)$$

where the weights $w_{\alpha} = \frac{e^{-S_{\text{OM}}[\mathbf{x}^{[\alpha]}]} \mathcal{Z}^{[\alpha]}}{\sum_{\gamma=1}^K e^{-S_{\text{OM}}[\mathbf{x}^{[\gamma]}]} \mathcal{Z}^{[\gamma]}}$ satisfy $\sum_{\alpha=1}^K w_{\alpha} = 1$, see the SI [27] for more details. Equation (4) is the infinite-dimensional analogue to approximating a finite-dimensional multimodal probability density by a sum of Gaussians, with one term for each local maximum of the probability density.

Transition channel probabilities. For temperature θ and path duration T we define $P^{[\alpha]}(\theta, T)$ as the probability of observing a transition path travelling via the α -th channel, i.e. close to the α -th instanton. Using Eq. (4) we approximate $P^{[\alpha]}(\theta, T)$ as

$$P^{[\alpha]}(\theta, T) \approx P_G^{[\alpha]}(\theta, T) \equiv \frac{e^{-S_{\text{OM}}[\mathbf{x}^{[\alpha]}]} \mathcal{Z}^{[\alpha]}}{\sum_{\gamma=1}^K e^{-S_{\text{OM}}[\mathbf{x}^{[\gamma]}]} \mathcal{Z}^{[\gamma]}}. \quad (5)$$

According to Eq. (5) the relative channel probabilities are determined by an interplay between the instanton probabilities, as quantified by $e^{-S_{\text{OM}}[\mathbf{x}^{[\alpha]}]}$, and the sizes of the Gaussian fluctuations around the local instantons, $\mathcal{Z}^{[\alpha]}$. It is instructive to compare this ratio with another estimator $P_I^{[\alpha]}(\theta, T) = \frac{e^{-S_{\text{OM}}[\mathbf{x}^{[\alpha]}]}}{\sum_{\gamma} e^{-S_{\text{OM}}[\mathbf{x}^{[\gamma]}]}}$, in which only the instanton probabilities are retained.

To use Eq. (5) in practice, we retrieve the instantons $\mathbf{x}^{[\alpha]}$ using a Ritz variational method presented in [33, 75]. We subsequently evaluate the regularised normalisation constants $\mathcal{Z}^{[\alpha]}$ using the Gelfand-Yaglom theorem [31, 65, 66, 68], as well as a generalisation thereof to non-gradient dynamics which we provide in the SI [27].

Numerical experiments. To infer the range of validity of our semi-analytical approximation it is necessary to compare Eq. (5) with numerical simulations. In parameter regimes where transitions are very rare, it is not feasible to sample the TPE using direct simulations. We therefore numerically probe the TPE using a MCMC algorithm built on the *pre-conditioned Crank-Nicholson algorithm* (pCN) [69–71], as detailed in the SI [27]. In essence, we approximate the function space of all transition paths by a finite sum of basis functions [39, 77, 78], and perform a random walk on the resulting finite-dimensional space of basis coefficients; the random walk is designed such that the resulting transition path samples are distributed according to the TPE we seek to probe.

A general shortcoming of MCMC methods and also other transition path sampling techniques [42–46] is that when the distribution to be sampled is multimodal with regions of low probability in between the modes, it may take prohibitively long to

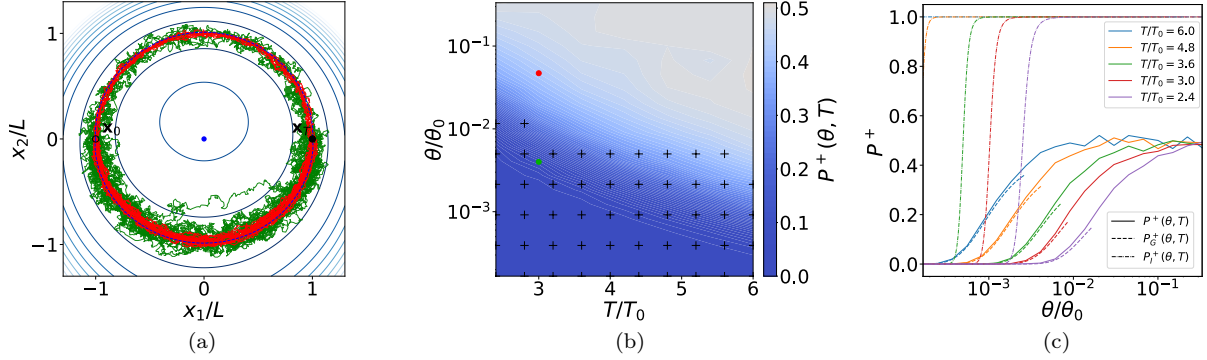


Figure 1. Diffusivity-dependence of the transition path ensemble for the conservative model system. Panel (a) shows 50 stochastic trajectories sampled using the TMC method (see text) for overdamped dynamics in the potential $U(x)$ [27]. The dashed blue (green) lines are upper (lower) instantons between initial (circle, \mathbf{x}_0) and final (filled circle, \mathbf{x}_T) points. Upper and lower channels are equally populated at temperature $\theta = 0.047\theta_0$ (green) but the lower channel is preferred at the lower temperature $\theta = 0.004\theta_0$ (red). Trajectories of duration $T = 3T_0$ are sampled with $N = 200(T/T_0)$ modes. Panel (b) is a pseudocolor plot quantifying the variation of the upper and lower channel probabilities with temperature and duration, as obtained from TMC. The plus signs show regions where the Gaussian mixture approximation P_G^+ , defined in Eq. (5), is within a 5% margin of error of the simulated value. The red and green dots correspond to the same color-coded simulations in panel (a). Panel (c) shows a comparison between the TMC, Gaussian mixture and instanton approximations to the upper channel probability as function of temperature for fixed durations of path.

obtain converged results. For overdamped Langevin dynamics Eq. (1), this corresponds to medium-to-low temperature regimes in systems with competing transition pathways, where the TPE concentrates around the local instantons. One way to overcome this issue is to use replica exchange [46], which requires running several instances of the MCMC algorithm at varying temperatures. Here we introduce a modification of the pCN-MCMC that operates only at one temperature, which we call the *Teleporter MCMC* (TMC), which utilises the Gaussian mixture approximation of the TPE. At each step of the TMC there is a small probability to jump between the transition channels, which accelerates mixing between them. We provide a detailed description of the algorithm in the SI [27].

Results. We now consider the transition behavior of the 2D system depicted in Fig. 1 (a). For a range of temperatures θ and total transition times T we first generate ensembles of 10^8 sample transition paths per tuple (θ, T) using the TMC. Let $\tau_D(\theta) = L^2/(\mu k_B \theta)$, which is the diffusive time-scale at temperature θ . We also introduce fixed reference temperature and time-scales $\theta_0 = U_0/k_B$ and $T_0 = \tau_D(\theta_0)$, where U_0 is the energetic well-depth of the potential. Our parameter range is such that $T \ll \tau_D$, for each temperature θ in the range considered. Each sampled ensemble thus describes a rare transition event. For a total transition time $T/T_0 = 3$, and for each of the two temper-

atures $\theta/\theta_0 = 0.047$ and $\theta/\theta_0 = 0.004$, we show 50 randomly chosen TMC sample paths in Fig. 1 (a). We observe that while for the higher temperature the paths are evenly distributed between the two channels, for the lower temperature the lower channel is preferred. In Fig. 1 (b) we show TMC results for $P^+(\theta, T) \equiv P^{[1]}(\theta, T)$, the probability of the upper channel, as a function of both θ and T . Consistent with the $\theta/\theta_0 = 0.047$ data from Fig. 1 (a), we observe that for large enough temperature $P^+(\theta, T) \approx 1/2$ (white region), so that upper and lower channel are equally probable. That at large temperature the asymmetry in U becomes irrelevant for the TPE is expected, as in this limit the random force in Eq. (1) dominates over the deterministic force. As θ is decreased, the channel around Γ^- becomes dominant, so that $P^+(\theta, T) \rightarrow 0$ (blue region in Fig. 1 (b), c.f. $\theta/\theta_0 = 0.004$ data in subplot (a)). The exact temperature at which the crossover from the diffusivity-dominated regime to the drift-dominated regime occurs decreases with increasing T ; this is clearly seen in Fig. 1 (c) where vertical sections of subplot (b) are shown for several values of T .

We now compare our numerical TMC results for $P^+(\theta, T)$ with the Gaussian mixture approximation $P_G^+(\theta, T) \equiv P_G^{[1]}(\theta, T)$, defined in Eq. (5). Figure 1 (b) shows that this approximation is valid in the low-temperature regime (plus signs). This is consistent with the assumptions underlying the Gaussian ap-

proximation, as we expect the probability distribution in path space to be dominated by the neighborhoods of the local instantons only for sufficiently low temperature. As Fig. 1 (c) shows, $P_G^+(\theta, T)$ quantitatively captures the beginning of the crossover from drift-dominated to diffusivity-dominated transition behaviour for all values of T considered.

For capturing this θ -dependent crossover, the prefactors $\mathcal{Z}^+ = \mathcal{Z}^{[1]}$, $\mathcal{Z}^- = \mathcal{Z}^{[2]}$ in Eq. (5) are essential. This becomes apparent by considering $P_I^+(\theta, T)$, which only depends on the relative probabilities of the two local instantons. In Fig. 1 (c) we see that for high enough temperatures $P_I^+(\theta, T) \approx 1$, meaning $S_{\text{OM}}[\mathbf{x}^+(t)] < S_{\text{OM}}[\mathbf{x}^-(t)]$ [47]. This limit is understood by comparing the two terms in the action Eq. (B5). While the first term scales as $1/\theta$, the second term is independent of θ ; for fixed T and large enough θ the second term thus dominates the action. This second term is smaller for the channel around Γ^+ than for the channel around Γ^- , because the former channel is narrower leading to a smaller value of $\nabla \cdot \mathbf{F}$. As θ is decreased for fixed T the first term in Eq. (B5) becomes dominant. Figure 1 (c) shows that this leads to a crossover to $P_I^+(\theta, T) \approx 0$, meaning \mathbf{x}^- becomes more probable than \mathbf{x}^+ . While this low-temperature limit is consistent with the numerical results, the temperature at which we observe the crossover in $P_I^+(\theta, T)$ is smaller as compared to $P^+(\theta, T)$. For example, we see in Fig. 1 (c) that for $T/T_0 = 2.4$ the crossover of $P_I^+(\theta, T)$ is at $\theta/\theta_0 < 10^{-2}$, whereas the crossover for $P^+(\theta, T)$ occurs at $\theta/\theta_0 > 10^{-2}$. In particular this implies that for $\theta/\theta_0 = 10^{-2}$ the most probable path goes along Γ^+ , while most transition paths go along Γ^- . This highlights that even at intermediate-to-low temperatures, where the Gaussian mixture approximation Eq. (5) is already valid, the probabilities of the local instantons alone are insufficient to obtain the actual transition behaviour. Instead it is the prefactors \mathcal{Z}^\pm in Eq. (5) that dominate the crossover behaviour in Fig. 1 (b); these Gaussian normalisation constants are, in a sense, an entropic contribution, as they measure the effective volume in path space of the support around the respective local instanton. Even though for $T/T_0 = 2.4$, $\theta/\theta_0 = 10^{-2}$ the instanton \mathbf{x}^+ is more probable than \mathbf{x}^- , this is more than offset by the larger number of paths that behave similar to \mathbf{x}^- . As we discuss in the SI [27], the prefactors \mathcal{Z}^\pm remain relevant even in the Freidlin-Wentzell-Graham limit [18, 20] of vanishing temperature and infinite path duration.

For non-gradient forms of the drift, the prefactors \mathcal{Z}^\pm can also drive the crossover behaviour of the system, as we show now by adding a force of strength

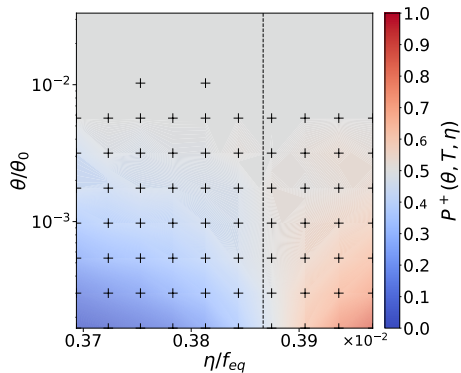


Figure 2. Diffusivity-dependence of the transition path ensemble for the non-conservative model system. Pseudocolour plot of the probability of the upper channel, $P^+(\theta, T, \eta)$, for the non-gradient system with $T/T_0 = 3$, as a function of the temperature θ and the circular force-strength η . The black plus signs show regions where the variational approximation $P_G^+(\theta, T, \eta)$, defined in Eq. (5), is within a 5% margin of error of the simulated value. The dashed line shows the crossover force strength $\eta_c/f_{\text{eq}} \approx 0.00387$, where f_{eq} is the characteristic strength of the gradient force [27].

η that acts perpendicular to the radius vector in the clockwise direction. For positive force strength η , this non-conservative force biases towards the upper channel Γ^+ . In Fig. 2 we show numerical results for $P^+(\theta, T, \eta)$ as a function of η and θ for $T/T_0 = 3$. For small $\eta/f_{\text{eq}} \rightarrow 0$, with f_{eq} the characteristic strength of the gradient force [27], we recover the results from Fig. 1 (b), (c). Thus at small but finite temperature the dominant transition channel is the one where particles travel against the weak non-conservative force. As η is increased to $\eta_c/f_{\text{eq}} \approx 0.00387$, we observe a crossover from Γ^- -channel dominated transitions to Γ^+ -channel dominated transitions in the low-temperature regime. This switch is also captured by the Gaussian approximation (plus signs in Fig. 2). On the other hand, throughout the parameter regime considered in Fig. 2, we find that $P_I^+(\theta, T, \eta) \approx 1$, meaning that the local instanton \mathbf{x}^+ is always more probable than \mathbf{x}^- for finite η . This again highlights the relevance of considering Gaussian fluctuations around the instantons for determining the dominant transition pathway.

Conclusion. For a system with two competing transition pathways, we have studied how the dominant transition pathway depends on both the temperature and the total duration. To quantify the relative importance of the competing pathways, we have constructed semi-analytical approximators which are valid in the low-to-intermediate temper-

ature regime. We have validated our approximators via comparison with a continuous-time MCMC method that is dimensionally robust and efficiently samples systems with multiple reactive pathways.

Our results show that even in the low-to-intermediate temperature regime the global instanton, or most probable path, itself is not sufficient to determine the dominant transition pathway. Rather, it is vital that fluctuations around this path be incorporated. This has a simple one-dimensional equivalent: For a probability density $\rho(x) \sim \exp(-V(x))$ for some potential $V(x)$ with relative minima x_α , the probabilistically most relevant minimum is not the global one, but that with the largest well probability, i.e. the x_α that maximizes $P(\text{well around } x_\alpha) \sim e^{-V(x_\alpha)} \sqrt{2\pi/V''(x_\alpha)}$, where we use a quadratic Taylor approximation of V around x_α . The most probable well is thus determined by an interplay of $e^{-V(x_\alpha)}$ (which corresponds to the instanton probability $e^{-S_{\text{OM}}[x^{[\alpha]}]}$) and $\sqrt{2\pi/V''(x_\alpha)}$ (which corresponds to the regularised normalisation constant $Z^{[\alpha]}$).

In the present paper we consider a paradigmatic example system with two competing transition pathways. The method of instantons is an established technique in theoretical chemistry and statistical physics [33, 48–55], and the method of Gaussian mixtures presented here scales as $O(d^2)$ with the number of degrees of freedom d [27]. It is therefore feasible to apply the methods we developed here to more realistic many-particle systems to study e.g. nucleation pathways [49, 56, 57] or conformational rearrangements in macromolecules [46, 58–60].

Our quantification here of the finite-temperature breakdown of instanton theories is important for relating such theories to experiments, which are always at finite temperatures. Our insights into path-space probability distributions for diffusive stochastic dynamics, together with our MCMC method, will therefore be valuable for going beyond the regime of asymptotically low diffusivity in both large deviations theory [18, 48, 51, 61] and the study of rare events [62].

Acknowledgements. We thank Professor M. E. Cates for many helpful discussions. Work funded in part by the European Research Council under the Horizon 2020 Programme, ERC grant agreement number 740269, and by the Royal Society through grant RP1700.

* ltk26@cam.ac.uk

- [1] N. G. V. Kampen, *Stochastic Processes in Physics and Chemistry* (Elsevier, 2011).
- [2] C. Gardiner, *Stochastic Methods: A Handbook for the Natural and Social Sciences* (Springer Berlin Heidelberg, 2010).
- [3] H. Risken and T. Frank, *The Fokker-Planck Equation: Methods of Solution and Applications* (Springer Science & Business Media, 2012).
- [4] A. T. Bharucha-Reid, *Elements of the Theory of Markov Processes and Their Applications* (Courier Corporation, 2012).
- [5] P. Faccioli, M. Sega, F. Pederiva, and H. Orland, *Physical Review Letters* **97**, 108101 (2006), arXiv:q-bio/0510045.
- [6] C. DeMarco, *IEEE Control Systems Magazine* **21**, 40 (2001).
- [7] T. S. Gardner, C. R. Cantor, and J. J. Collins, *Nature* **403**, 339 (2000).
- [8] M. Mangel, *Theoretical Population Biology* **45**, 16 (1994).
- [9] P. G. Wolynes, J. N. Onuchic, and D. Thirumalai, *Science* (1995), 10.1126/science.7886447.
- [10] S. Huang, *BioEssays: News and Reviews in Molecular, Cellular and Developmental Biology* **34**, 149 (2012).
- [11] L. Paninski, *Journal of Computational Neuroscience* **21**, 71 (2006).
- [12] B. C. Nolting and K. C. Abbott, *Ecology* **97**, 850 (2016).
- [13] J. Lee, I.-H. Lee, I. Joung, J. Lee, and B. R. Brooks, *Nature Communications* **8**, 15443 (2017).
- [14] L. Onsager and S. Machlup, *Physical Review* **91**, 1505 (1953).
- [15] A. Bach, D. Dürr, and B. Stawicki, *Zeitschrift für Physik B Condensed Matter and Quanta* **26**, 191 (1977).
- [16] H. Ito, *Progress of Theoretical Physics* **59**, 725 (1978).
- [17] N. Ikeda and S. Watanabe, *Stochastic Differential Equations and Diffusion Processes* (Elsevier, 2014).
- [18] A. D. Ventsel' and M. I. Freidlin, *Russian Mathematical Surveys* **25**, 1 (1970).
- [19] R. L. Stratonovich, in *Noise in Nonlinear Dynamical Systems: Volume 1: Theory of Continuous Fokker-Planck Systems*, Vol. 1, edited by F. Moss and P. V. E. McClintock (Cambridge University Press, Cambridge, 1989) pp. 16–71.
- [20] R. Graham, in *Noise in Nonlinear Dynamical Systems: Volume 1: Theory of Continuous Fokker-Planck Systems*, Vol. 1, edited by F. Moss and P. V. E. McClintock (Cambridge University Press, Cambridge, 1989) pp. 225–278.
- [21] L. Arnold, *Stochastic Differential Equations: Theory and Applications* (Wiley, 1974).
- [75] J. Gladrow, U. F. Keyser, R. Adhikari, and J. Kappler, *Physical Review X* **11**, 031022 (2021).
- [68] I. M. Gel'fand and A. M. Yaglom, *Journal of Mathematical Physics* **1**, 48 (1960).
- [24] D. Nickelsen and H. Touchette, *Physical Review E* **105**, 064102 (2022).
- [25] G. Corazza and M. Fadel, arXiv:2004.06654 [cond-

- mat, physics:math-ph] (2020), arXiv: 2004.06654.
- [26] Y. Lu, A. Stuart, and H. Weber, *SIAM Journal on Mathematical Analysis* **49**, 3005 (2017).
- [27] See the supplementary information.
- [72] Y. Takahashi and S. Watanabe, in *Stochastic Integrals*, Lecture Notes in Mathematics, edited by D. Williams (Springer, Berlin, Heidelberg, 1981) pp. 433–463.
- [29] E. Engel and R. M. Dreizler, *Density Functional Theory: An Advanced Course* (Springer Science & Business Media, 2011).
- [30] I. M. Gelfand and S. V. Fomin, *Calculus of Variations* (Courier Corporation, 2012).
- [31] G. Corazza and M. Fadel, *Physical Review E* **102**, 022135 (2020).
- [67] A. Gelman, J. B. Carlin, H. S. Stern, and D. B. Rubin, *Bayesian Data Analysis* (Chapman and Hall/CRC, 1995).
- [33] L. Kikuchi, R. Singh, M. E. Cates, and R. Adhikari, *Physical Review Research* **2**, 033208 (2020).
- [66] G. V. Dunne, *Journal of Physics A: Mathematical and Theoretical* **41**, 304006 (2008), arXiv:0711.1178.
- [65] S. Levit and U. Smilansky, *Proceedings of the American Mathematical Society* **65**, 299 (1977).
- [70] S. L. Cotter, G. O. Roberts, A. M. Stuart, and D. White, *Statistical Science* **28**, 424 (2013).
- [69] A. Beskos, G. Roberts, A. Stuart, and J. Voss, *Stochastics and Dynamics* **08**, 319 (2008).
- [71] M. Hairer, A. M. Stuart, and S. J. Vollmer, *The Annals of Applied Probability* **24**, 2455 (2014).
- [39] Kosambi, *Journal of the Indian Mathematical Society* **7**, 76 (1943).
- [77] K. Karhunen, *Über lineare Methoden in der Wahrscheinlichkeitsrechnung.*, Ph.D. thesis, Universitat Helsinki, Helsinki (1947).
- [78] M. Loève, *Probability Theory I*, 4th ed., Graduate Texts in Mathematics, Vol. 45 (Springer-Verlag, New York, 1977).
- [42] P. G. Bolhuis, D. Chandler, C. Dellago, and P. L. Geissler, *Annual Review of Physical Chemistry* **53**, 291 (2002).
- [43] P. G. Bolhuis and D. W. H. Swenson, *Advanced Theory and Simulations* **4**, 2000237.
- [44] C. Dellago, P. G. Bolhuis, F. S. Csajka, and D. Chandler, *The Journal of Chemical Physics* **108**, 1964 (1998).
- [45] C. Dellago, P. G. Bolhuis, and D. Chandler, *The Journal of Chemical Physics* **108**, 9236 (1998).
- [46] H. Fujisaki, M. Shiga, and A. Kidera, *The Journal of Chemical Physics* **132**, 134101 (2010).
- [47] A. B. Adib, *The Journal of Physical Chemistry B* **112**, 5910 (2008), arXiv:0712.1255.
- [48] W. E, W. Ren, and E. Vanden-Eijnden, *Communications on Pure and Applied Mathematics* **57**, 637 (2004).
- [49] W. E, W. Ren, and E. Vanden-Eijnden, *Physical Review B* **66**, 052301 (2002).
- [50] T. Grafke, R. Grauer, and T. Schäfer, *Journal of Physics A: Mathematical and Theoretical* **48**, 333001 (2015).
- [51] T. Grafke and E. Vanden-Eijnden, *Chaos: An Interdisciplinary Journal of Nonlinear Science* **29**, 063118 (2019).
- [52] T. Schorlepp, T. Grafke, and R. Grauer, *Journal of Physics A: Mathematical and Theoretical* (2021), 10.1088/1751-8121/abfb26.
- [53] G. Dematteis, T. Grafke, M. Onorato, and E. Vanden-Eijnden, *Physical Review X* **9**, 041057 (2019).
- [54] G. Ferré and T. Grafke, arXiv:2011.10990 [cond-mat] (2021), arXiv:2011.10990 [cond-mat].
- [55] M. Heymann and E. Vanden-Eijnden, *Communications on Pure and Applied Mathematics* **61**, 1052 (2008).
- [56] J. F. Lutsko, *Science Advances* (2019), 10.1126/sciadv.aav7399.
- [57] P. Rein ten Wolde, M. J. Ruiz-Montero, and D. Frenkel, *The Journal of Chemical Physics* **104**, 9932 (1996).
- [58] W. Ren, E. Vanden-Eijnden, P. Maragakis, and W. E, *The Journal of Chemical Physics* **123**, 134109 (2005).
- [59] H. Fujisaki, M. Shiga, K. Moritsugu, and A. Kidera, *The Journal of Chemical Physics* **139**, 054117 (2013).
- [60] T. E. Gartner and A. Jayaraman, *Macromolecules* **52**, 755 (2019).
- [61] E. Vanden-Eijnden and M. Heymann, *The Journal of Chemical Physics* **128**, 061103 (2008).
- [62] T. Grafke, T. Schäfer, and E. Vanden-Eijnden, arXiv:2103.04837 [cond-mat, physics:physics] (2021), arXiv:2103.04837 [cond-mat, physics:physics].
- [63] L. Gross, in *Proceedings of the Fifth Berkeley Symposium on Mathematical Statistics and Probability, Volume 2: Contributions to Probability Theory, Part 1*, Berkeley Symposium on Mathematical Statistics and Probability, Vol. 5.2A (University of California Press, California, 1967) pp. 31–42.
- [64] C. Dewitt-Morette and A. Folacci, *Functional Integration: Basics and Applications* (Springer Science & Business Media, 2013).
- [65] S. Levit and U. Smilansky, *Proceedings of the American Mathematical Society* **65**, 299 (1977).
- [66] G. V. Dunne, *Journal of Physics A: Mathematical and Theoretical* **41**, 304006 (2008), arXiv:0711.1178.
- [67] A. Gelman, J. B. Carlin, H. S. Stern, and D. B. Rubin, *Bayesian Data Analysis* (Chapman and Hall/CRC, 1995).
- [68] I. M. Gelfand and A. M. Yaglom, *Journal of Mathematical Physics* **1**, 48 (1960).
- [69] A. Beskos, G. Roberts, A. Stuart, and J. Voss, *Stochastics and Dynamics* **08**, 319 (2008).
- [70] S. L. Cotter, G. O. Roberts, A. M. Stuart, and D. White, *Statistical Science* **28**, 424 (2013).
- [71] M. Hairer, A. M. Stuart, and S. J. Vollmer, *The Annals of Applied Probability* **24**, 2455 (2014).
- [72] Y. Takahashi and S. Watanabe, in *Stochastic Integrals*, Lecture Notes in Mathematics, edited by D. Williams (Springer, Berlin, Heidelberg, 1981) pp. 433–463.

- [73] H. Ito, *Progress of Theoretical Physics* **59**, 725 (1978).
- [74] G. A. Pavliotis, *Stochastic Processes and Applications: Diffusion Processes, the Fokker-Planck and Langevin Equations* (Springer New York, 2014).
- [75] J. Gladrow, U. F. Keyser, R. Adhikari, and J. Kappler, *Physical Review X* **11**, 031022 (2021).
- [76] D. D. Kosambi, in *Ramaswamy R. (Eds) D.D. Kosambi* (Springer, New Delhi, 2016) pp. 59–70.
- [77] K. Karhunen, *Über lineare Methoden in der Wahrscheinlichkeitsrechnung.*, Ph.D. thesis, Universität Helsinki, Helsinki (1947).
- [78] M. Loève, *Probability Theory I*, 4th ed., Graduate Texts in Mathematics, Vol. 45 (Springer-Verlag, New York, 1977).

Appendix A: System specification

Here we define the two systems in consideration in the main text. We construct a Sombbrero-type potential such that the perpendicular curvature of the potential along the minimal upper semi-circle Γ^+ is larger than that along the lower semi-circle Γ^- . We start with a radial quartic potential of the form

$$U(x_1, x_2) = U_r(r(x_1, x_2)) \quad (\text{A1})$$

$$U_r(r) = U_0 \left(\frac{r}{L} - 1 \right) \left(1 + a \frac{r}{L} + b \left(\frac{r}{L} \right)^2 + c \left(\frac{r}{L} \right)^3 \right)$$

where L is the length-scale of the system, U_0 will be the value of the potential at the local maximum $r = 0$, and $a, b, c \in \mathbb{R}$ will be specified below. We will henceforth suppress the argument of the radial coordinate function $r(x_1, x_2) = \sqrt{x_1^2 + x_2^2}$. Let $\Gamma = \{(x, y) \mid r = 1\}$ be the circle centered around the origin, which satisfies $U_r(1) = 0$. We also define Γ^+ and Γ^- as the upper and lower semi-circle respectively. We impose the following conditions on the potential to fix a, b, c :

1. $U'_r(0) = 0$. The origin is an extremum.
2. $U'_r(1) = 0$. Γ is an extremum of the potential.
3. $U''_r(1) = k$. The curvature along Γ is k .

We get

$$U_r(r) = \frac{1}{2} \left(\frac{r}{L} - 1 \right)^2 \left[L^2 k \left(\frac{r}{L} \right)^2 - 2U_0 \left(\frac{r}{L} - 1 \right) \left(3 \frac{r}{L} + 1 \right) \right] \quad (\text{A2})$$

In order to ensure that the potential has a Sombbrero-like form, we must further have that the potential is confining, which is equivalent to $\lim_{r \rightarrow \infty} U_r(r) = \infty$, which implies that $6U_0 \leq L^2 k$. We now introduce an angular dependence in the curvature. We set

$$L^2 k(\phi) = 6U_0(1 + 2h(\phi)) \quad (\text{A3})$$

where $\phi = \phi(x_1, x_2)$ is the angle of (x_1, x_2) in polar coordinates so that $x_1 = \cos(\phi)$, $x_2 = \sin(\phi)$, and where

$$h(\phi) = \frac{1}{4} (\xi_2 + \xi_1 + (\xi_2 - \xi_1) \sin \phi) \quad (\text{A4})$$

where $\xi_2 > \xi_1$, and where $h(\phi) \in [\xi_1, \xi_2]$ satisfies $h(-\pi/2) = \xi_1$ and $h(\pi/2) = \xi_2$. Eq. (A3) is constructed so that the perpendicular curvature of Γ^+ is larger than that of Γ^- . The drift of the system is now given by $\mathbf{F} = -\nabla U$.

For the non-gradient system, we introduce an additional non-conservative force $\mathbf{F}^a = -\eta \hat{\phi}$ for which the work done in a displacement $d\mathbf{x} = dr\hat{\mathbf{r}} + rd\phi\hat{\phi}$ is $dW = \mathbf{F}^a \cdot d\mathbf{x} = \eta r d\phi$. This force energetically biases the upper transition channel Γ^+ . The total force is thus $\mathbf{F} = -\nabla U + \mathbf{F}^a$.

In the numerical experiments presented in the main text, we used the Itô Langevin equation

$$d\mathbf{X} = \mu \mathbf{F} dt + \sqrt{2\mu k_B \theta} d\mathbf{W}. \quad (\text{A5})$$

We now put Eq. A5 in non-dimensionalised form by introducing the time-scale $T_0 = \frac{L^2}{k_B\theta_0\mu}$ and temperature-scale θ_0 , and setting $t = T_0\tilde{t}$, $\theta = \theta_0\tilde{\theta}$, $\mathbf{X} = L\tilde{\mathbf{X}}$, $\mathbf{F} = \frac{U_0}{L}\tilde{\mathbf{F}}$ and $\mathbf{W} = \sqrt{T_0}\tilde{\mathbf{W}}$. T_0 is the typical diffusion time-scale at temperature θ_0 . We get

$$d\tilde{\mathbf{X}} = \tilde{U}_0\tilde{\mathbf{F}}d\tilde{t} + \sqrt{2\tilde{\theta}}d\tilde{\mathbf{W}}.$$

where $\tilde{U}_0 = \frac{U_0}{k_B\theta_0}$ is the ratio of the well-depth U_0 and the thermal energy at temperature θ_0 . For the numerical experiments in the main text we use $\tilde{U}_0 = 1$, which means that $\tilde{\theta} = 1$ corresponds to a temperature such that $k_B\theta = U_0$. We also set $\xi_1 = 0$ and $\xi_2 = 2$. To compare the gradient force with \mathbf{F}^a we also introduce $f_{\text{eq}} = U_0/L$, which is the characteristic force strength of the gradient force.

Appendix B: Gaussian mixture approximation of the transition path ensemble

Here we derive an approximation of the transition path ensemble, using a Gaussian mixture approximation of the path-space probability measure. The subsequent sections give detailed descriptions of the mathematical techniques necessary for the approximation, but we will first give some intuition by drawing an analogy to a one-dimensional probability density.

For a one-dimensional probability density $\rho(x) = \mathcal{N}^{-1} \exp(-V(x))$, where \mathcal{N} is a normalization constant and where the potential $V(x)$ has well-separated relative minima x_α , $\alpha = 1, \dots, K$, we can approximate $\rho(x)$ around x_α using a Gaussian approximation

$$\rho(x) \approx \frac{1}{\mathcal{N}} e^{-V(x_\alpha) - V''(x_\alpha)(x-x_\alpha)^2/2} =: \frac{\mathcal{N}_\alpha}{\mathcal{N}} e^{-V(x_\alpha)} \rho^{[\alpha]}(x) \quad (\text{B1})$$

with a normalised Gaussian distribution $\rho^{[\alpha]}(x) := \mathcal{N}_\alpha^{-1} e^{-V''(x_\alpha)(x-x_\alpha)^2/2}$ and where $\mathcal{N}_\alpha = \sqrt{2\pi/V''(x_\alpha)}$. Equation B1 is a local approximation of $\rho(x)$ around x_α . If $\rho(x)$ is highly peaked around its maxima (for example if $V(x)$ describes a Boltzmann distribution $V(x) = U(x)/(k_B\theta)$ at a low temperature θ), a global approximation of $\rho(x)$ is the Gaussian mixture

$$\rho(x) \approx \sum_{\alpha=1}^K \frac{\mathcal{N}_\alpha}{\mathcal{N}} e^{-V(x_\alpha)} \rho^{[\alpha]}(x) =: \sum_{\alpha=1}^K w_\alpha \rho^{[\alpha]}(x) \quad (\text{B2})$$

where $w_\alpha = e^{-V(x_\alpha)}\mathcal{N}_\alpha/\mathcal{N}$ are constants that weight the local Gaussian distributions, and where $\mathcal{N} \approx \sum_{\gamma=1}^K e^{-V(x_\gamma)}\mathcal{N}_\gamma$.

Equation (B2) can be used to approximately evaluate any expectation value. In particular, the probability of being in well α (i.e. around x_α) is given by

$$P(x \in \text{well } \alpha) = \mathbb{E}[\chi_\alpha] = \int_{-\infty}^{\infty} dx \chi_\alpha(x) \rho(x) \approx \sum_{\beta=1}^K w_\beta \int_{-\infty}^{\infty} dx \chi_\alpha(x) \rho^{[\beta]}(x) \quad (\text{B3})$$

$$\approx w_\alpha \int_{-\infty}^{\infty} dx \rho^{[\alpha]}(x) = w_\alpha = \frac{e^{-V(x_\alpha)}\mathcal{N}_\alpha}{\sum_{\gamma=1}^L e^{-V(x_\gamma)}\mathcal{N}_\gamma}, \quad (\text{B4})$$

where the indicator function $\chi_\alpha(x)$ is 1 if x is in well α and zero otherwise, and where we assume that the potential wells of $V(x)$ are well-separated so that $\chi_\alpha(x)\rho^{[\beta]}(x)$ is negligibly small whenever $\alpha \neq \beta$.

In the following we apply the same steps as above to the case of the transition path ensemble (TPE). As we are considering Gaussian approximations of probability distributions over infinite-dimensional functional spaces, the mathematical sophistication required is higher, but the intuition remains identical to the above one-dimensional example. In Sec. II.A we derive the local Gaussian approximation for path-probability measures around an instanton (which is based on a second-order functional Taylor approximation), which we in Sec. II.B combine to a Gaussian mixture approximation of the TPE. In Sec. II.D we derive the method we use to calculate the normalisation constants for functional Gaussians (i.e. the infinite-dimensional equivalent

of the \mathcal{N}_α from the one-dimensional example above). We put Sec. II.D last as it is a technical result, and is not required to understand the rest of the subsections. In Sec. II.C we use the Gaussian mixture to derive an approximate expression for transition pathway probabilities, which proceeds analogous to the calculation Eq. (B4).

1. The quadratic expansion of the Onsager-Machlup action

Here we describe how to formally construct the Gaussian expansion around a given reference path. The variational expansion of the Onsager-Machlup action

$$S_{\text{OM}}[\mathbf{x}(t)] = \int_0^T L(\mathbf{x}(t), \dot{\mathbf{x}}(t)) dt \quad (\text{B5})$$

$$L(\mathbf{x}, \dot{\mathbf{x}}) = \frac{\beta}{4\mu} |\dot{\mathbf{x}} - \mathbf{F}|^2 + \frac{\mu}{2} \nabla \cdot \mathbf{F}$$

where $\beta = 1/k_B\theta$ is the inverse temperature, is given by

$$S_{\text{OM}}[\bar{\mathbf{x}} + \delta\mathbf{x}] = S_{\text{OM}}[\bar{\mathbf{x}}] + \mathbf{J}[\delta\mathbf{x}] + \frac{1}{2}\mathbf{H}[\delta\mathbf{x}] + O(\delta\mathbf{x}^3) \quad (\text{B6})$$

to second order around a reference path $\bar{\mathbf{x}}(t)$, where

$$\mathbf{J}[\delta\mathbf{x}] = \int_0^T \left\{ \frac{\partial L}{\partial \mathbf{x}}(\bar{\mathbf{x}}, \dot{\bar{\mathbf{x}}}) \cdot \delta\mathbf{x} + \frac{\partial L}{\partial \dot{\mathbf{x}}}(\bar{\mathbf{x}}, \dot{\bar{\mathbf{x}}}) \cdot \delta\dot{\mathbf{x}} \right\} dt \quad (\text{B7})$$

$$\mathbf{H}[\delta\mathbf{x}] = \int_0^T \left\{ \delta\mathbf{x} \cdot \frac{\partial^2 L}{\partial \mathbf{x} \partial \mathbf{x}}(\bar{\mathbf{x}}, \dot{\bar{\mathbf{x}}}) \cdot \delta\mathbf{x} + 2 \delta\mathbf{x} \cdot \frac{\partial^2 L}{\partial \mathbf{x} \partial \dot{\mathbf{x}}}(\bar{\mathbf{x}}, \dot{\bar{\mathbf{x}}}) \cdot \delta\dot{\mathbf{x}} + \delta\dot{\mathbf{x}} \cdot \frac{\partial^2 L}{\partial \dot{\mathbf{x}} \partial \dot{\mathbf{x}}}(\bar{\mathbf{x}}, \dot{\bar{\mathbf{x}}}) \cdot \delta\dot{\mathbf{x}} \right\} dt. \quad (\text{B8})$$

In the following we will suppress the arguments of the derivatives of the Lagrangian. We will now recast Eq. (B6) in terms of self-adjoint operators using integration-by-parts and $\delta\mathbf{x}(0) = \delta\mathbf{x}(T) = 0$. We also note that $\langle \mathbf{f}, P \frac{d}{dt} \mathbf{g} \rangle = -\langle \frac{d}{dt} (P^T \mathbf{f}), \mathbf{g} \rangle$, for any matrix function $P(t) \in \mathbb{R}^{d \times d}$, and where $\langle \mathbf{f}, \mathbf{g} \rangle = \sum_i \int_0^T f_i(t) g_i(t) dt$, which we use to symmetrise the second term in Eq. (B8). We get

$$S_{\text{OM}}[\bar{\mathbf{x}} + \delta\mathbf{x}] = S_{\text{OM}}[\bar{\mathbf{x}}(t)] + \langle \mathbf{j}, \delta\mathbf{x} \rangle + \frac{1}{2} \langle \delta\mathbf{x}, \mathcal{H} \delta\mathbf{x} \rangle + O(\delta\mathbf{x}^3) \quad (\text{B9})$$

where

$$\mathbf{j}(t) = \frac{\partial L}{\partial \mathbf{x}} - \frac{d}{dt} \frac{\partial L}{\partial \dot{\mathbf{x}}} \quad (\text{B10})$$

$$\mathcal{H} = -\frac{\beta}{2\mu} \frac{d^2}{dt^2} + 2A(t) \frac{d}{dt} + B(t) \quad (\text{B11})$$

and $A_{ij}(t) = \frac{\partial^2 L}{\partial x_i \partial \dot{x}_j}$, $B_{ij}(t) = \frac{\partial^2 L}{\partial x_i \partial x_j} - \frac{d}{dt} \frac{\partial^2 L}{\partial x_j \partial \dot{x}_i}$, where closed brackets indicate an anti-symmetrisation over indices. By completing the square, we find that Eq. (B9) defines a Gaussian process $\delta\mathbf{x} \sim \mathcal{N}(-\mathcal{H}^{-1}\mathbf{j}, \mathcal{H}^{-1})$, which describes the quadratic fluctuations around $\bar{\mathbf{x}}$. In the sense of [63], the path-space density of the Gaussian process is $\rho[\delta\mathbf{x}] \propto \exp(-\frac{1}{2} \langle \delta\mathbf{x} + \mathcal{H}^{-1}\mathbf{j}, \mathcal{H}(\delta\mathbf{x} + \mathcal{H}^{-1}\mathbf{j}) \rangle)$. If the reference path solves the Euler-Lagrange equation Eq. (B5), then $\mathbf{j} = 0$ and the Gaussian process simplifies to $\rho[\delta\mathbf{x}] \propto \exp(-\frac{1}{2} \langle \delta\mathbf{x}, \mathcal{H} \delta\mathbf{x} \rangle)$.

For systems with gradient dynamics $\mathbf{F} = -\nabla U$, the asymmetric term in Eq. (B11) vanishes, and the form of the operator simplifies to

$$\mathcal{H} = -\frac{\beta}{2\mu} \frac{d^2}{dt^2} + B(t) \quad (\text{B12})$$

2. Gaussian mixture approximation

We now use the quadratic expansion of the Onsager-Machlup action to construct an approximate probability measure over the TPE. Let $\mathbf{x}^{[\alpha]}, \alpha = 1, \dots, K$ be the local instantons of a given Langevin system. For each local instanton we can define a Gaussian measure $\mathbb{P}^{[\alpha]}$ with mean $\mathbf{x}^{[\alpha]}$ and precision $H^{[\alpha]}$. Although the measure $\mathbb{P}^{[\alpha]}$ is defined over the space of C^0 continuous paths, the distribution can be characterised via a density on the Hilbert space of C^2 paths as $\rho^{[\alpha]}[\mathbf{x}] \propto \exp(-\langle \mathbf{x} - \mathbf{x}^{[\alpha]}, \mathcal{H}^{[\alpha]}(\mathbf{x} - \mathbf{x}^{[\alpha]}) \rangle)$ [63, 64]. To approximate the TPE distribution, we construct the mixed Gaussian density $\bar{\rho}[\mathbf{x}] \propto \sum_{\alpha=1}^K e^{-S_{\text{OM}}[\mathbf{x}^{[\alpha]}]} \rho^{[\alpha]}[\mathbf{x}]$. The normalisation constant $\mathcal{N}^{[\alpha]}$ of the densities $\rho^{[\alpha]}[\mathbf{x}]$ are not finite, but can be expressed as ratios with respect to the normalisation of the reference Wiener measure \mathcal{N}^W . This ratio can be shown to be equal to [65, 66]

$$\mathcal{Z}^{[\alpha]} := \frac{\mathcal{N}^{[\alpha]}}{\mathcal{N}^W} = \left(\frac{\det[\mathcal{H}^{[\alpha]}]}{\det[-\frac{\beta}{2\mu} \frac{d^2}{dt^2}]} \right)^{-1/2} \quad (\text{B13})$$

where the RHS can be computed using the results in the Sec. II-C. Using Eq. (B13) we can write down the approximation of the TPE as the Gaussian mixture [67]

$$\bar{\mathbb{P}} = \sum_{\alpha=1}^K w_{\alpha} \mathbb{P}^{[\alpha]} \quad (\text{B14})$$

where $w_{\alpha} = e^{-S_{\text{OM}}[\mathbf{x}^{[\alpha]}]} \mathcal{Z}^{[\alpha]} / \sum_{\gamma=1}^K e^{-S_{\text{OM}}[\mathbf{x}^{[\gamma]}]} \mathcal{Z}^{[\gamma]}$.

3. Approximations of transition channel probabilities

We now derive an approximation to the probabilities of reactive pathways using the Gaussian mixture approximation of the TPE. Let $E_{\alpha} \subset C^0, \alpha = 1, \dots, K$, which are disjoint open sets in the TPE, be the K reactive pathways under consideration. We define the observable

$$P^{[\alpha]}(\theta, T) = \mathbb{P}[E_{\alpha}] \quad (\text{B15})$$

which is the probability of observing a path in E_{α} . In low temperatures we can assume that $\mathbb{P}(\cup_{\alpha} E_{\alpha}) \approx 1$, i.e. approximately all stochastic paths transition via one of the reactive pathways. Furthermore, we assume that $\mathbf{x}^{[\alpha]} \in E_{\alpha}$ and that $\mathbb{P}^{[\alpha]}(\cup_{\gamma \neq \alpha} E_{\gamma}) \approx 0$. The latter assumption means that each measure $\mathbb{P}^{[\alpha]}$ is concentrated on E_{α} and lacks support on the other reactive pathways. Under these assumptions we can approximate $P^{[\alpha]}(\theta, T)$ as

$$P^{[\alpha]}(\theta, T) \approx P_G^{[\alpha]}(\theta, T) \equiv w_{\alpha}. \quad (\text{B16})$$

4. Calculation of the Gaussian normalisation constants

The regularised normalisation constants of Gaussians defined on functional spaces can be found by computing the determinants of their covariance operators. Equivalently, the normalisation can be found by computing the determinant of their precision operator, which is the inverse of the covariance operator. As for finite-dimensional linear operators, determinants of differential operators can be found by computing their eigenvalues, but this is in general a prohibitively expensive computational procedure. In the following we show that functional determinants, acting on d -dimensional vectors, can be found by solving d initial value ODEs.

Let the linear operators

$$\mathcal{L} = \frac{d}{dt} \left(P \frac{d}{dt} \right) - R \quad (\text{B17})$$

and

$$\mathcal{L}_0 = \frac{d}{dt} \left(P \frac{d}{dt} \right) \quad (\text{B18})$$

be defined for $0 \leq t \leq T$, and where $P(t) \in \mathbb{R}^{d \times d}$ is a positive-definite matrix function and $R(t) \in \mathbb{R}^{d \times d}$ is a matrix function. Let $\gamma^{(k)}$ and $\mathbf{u}^{(k)}(t; \alpha)$ be the eigenvalues and eigenfunctions of \mathcal{L} , which are solutions to the boundary value problem

$$\mathcal{L}\mathbf{u}^{(k)}(t) = \gamma^{(k)}\mathbf{u}^{(k)}(t) \quad (\text{B19})$$

where $\mathbf{u}^{(k)}(0) = \mathbf{u}^{(k)}(T) = 0$. Similarly, let $\mathbf{u}_0^{(k)}(t)$ and $\gamma_0^{(k)}$ be the eigenfunctions and eigenvalues of \mathcal{L}_0 . Then the *functional determinant* of \mathcal{L} is defined in regularised form as

$$\frac{\det \mathcal{L}}{\det \mathcal{L}_0} = \prod_{k=1}^{\infty} \frac{\gamma^{(k)}}{\gamma_0^{(k)}}. \quad (\text{B20})$$

As the spectrum of Eq. (B17) is unknown, and numerically expensive to compute, a much more efficient way of computing Eq. (B20) is via the Gelfand-Yaglom theorem (GYT) [65, 66, 68]. The GYT states that the functional determinant can be expressed as

$$\left| \frac{\det \mathcal{L}}{\det \mathcal{L}_0} \right| = \left| \frac{\det [Y(T)]}{\det [Y_0(T)]} \right| \quad (\text{B21})$$

where $Y(t) \in \mathbb{R}^{d \times x}$ with components $Y_{ij}(t) = y_i^{(j)}(t)$, where the $\mathbf{y}^{(j)}(t)$ are solutions to the d second-order ODEs with initial conditions

$$\mathcal{L}\mathbf{y}^{(j)}(t) = 0 \quad (\text{B22})$$

$$\mathbf{y}^{(j)}(0) = 0 \quad (\text{B23})$$

$$\frac{d}{dt} y_i^{(j)}(0) = \delta_{ij}. \quad (\text{B24})$$

and where the matrix $Y_0(t) \in \mathbb{R}^{d \times d}$ is defined similarly, but with \mathcal{L} in Eq. (B22) replaced with \mathcal{L}_0 .

In the case of gradient dynamics, where \mathcal{H} takes the form in Eq. (B12), the GYT can be readily applied by setting $P(t) = -\frac{\beta}{2\mu} I_d$ and $R(t) = -B(t)$, where I_d is the identity matrix. We now present a generalisation of the GYT that allows for linear operators of the form

$$\mathcal{L} = \frac{d^2}{dt^2} + U \frac{d}{dt} + R \quad (\text{B25})$$

where $0 \leq t \leq T$, and where $U(t)$, $R(t) \in \mathbb{R}^{d \times d}$ are matrix functions, which then makes the GYT applicable for systems non-gradient dynamics, with precision operators of the form Eq. (B11).

We define the linear operator \mathcal{G} which acts on vector functions as

$$\mathcal{G}\mathbf{y} = G\mathbf{y}$$

where $G(t)$ is a matrix function that solves the equation

$$\dot{G} = -\frac{1}{2}UG, \quad (\text{B26})$$

then the linear operator

$$\tilde{\mathcal{L}} = \mathcal{G}^{-1}\mathcal{L}\mathcal{G} = \frac{d}{dt^2} + G^{-1} \left(R - \frac{1}{2}\dot{U} - \frac{1}{4}U^2 \right) G \quad (\text{B27})$$

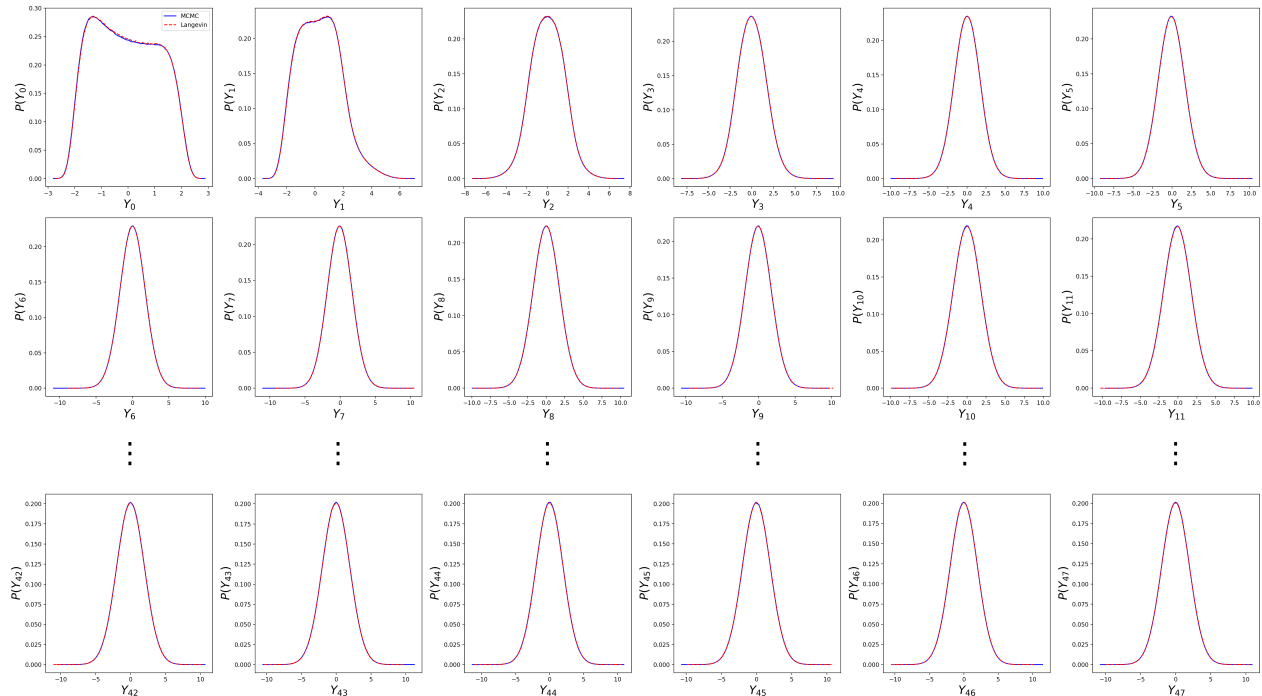


Figure 3. The marginalised distributions of the of the modes of the sample paths of an asymmetric double well system, generated by the MCMC method (blue) and an Euler-Mayurama direct integrator (red) in the KKL basis, at $\theta/\theta_0 = 1.69$, $T/T_0 = 3.33$ and $N = 200(T/T_0)$.

is of the form Eq. (B17) and $\det \tilde{\mathcal{L}}$ can then be computed using the GYT. As for any two operators \mathcal{A} and \mathcal{B} , we have that $\det \mathcal{A}\mathcal{B} = \det \mathcal{A} \det \mathcal{B}$, and $\det \mathcal{A}^{-1} = 1/\det \mathcal{A}$, and we therefore have that $\det \mathcal{L} = \det \tilde{\mathcal{L}}$. The functional determinant $\det \mathcal{L}$ can thus be computed by first solving Eq. (B26), constructing $\tilde{\mathcal{L}}$ using Eq. (B27), and finally using the GYT to compute $\det \tilde{\mathcal{L}}$.

The above theorem can be applied to Eq. (B11) by setting $P(t) = -\frac{\beta}{2\mu} I_d$, $U = -\frac{4\mu}{\beta} A$ and $R = B$. Using the GYT, and its generalisation presented here, the problem of computing the normalisation constants of Gaussian distributions in functional spaces is reduced to solving d initial value problems.

Appendix C: MCMC method

Here we define the MCMC method used to validate the semi-analytical results on the transition path ensemble. We start with an introduction to the *preconditioned Crank-Nicholson* algorithm [69–71], and MCMC in continuous time. This is followed by a description of the *Teleporter MCMC*, which is the algorithm we use to sample the systems introduced in the main text.

1. MCMC in continuous time

The Onsager-Machlup action Eq. (B5) can be interpreted as a fictitious density $P[\mathbf{x}(t)] \propto \exp(-S_{\text{OM}}[\mathbf{x}(t)])$ with respect to a fictitious Lebesgue measure on the space of continuous paths [72][63, 64]. This interpretation is however not mathematically rigorous: Neither does an infinite-dimensional Lebesgue measure exist, nor is the Onsager-Machlup action well defined for stochastic paths, which is because the temporal integral over the term proportional to \dot{x}^2 diverges for a stochastic path (which is typically nowhere differentiable). Both these mathematical issues are fixed by absorbing the term proportional to \dot{x}^2 into the measure, so that the path probability measure \mathbb{P} is described through its density *with respect to* the Wiener measure \mathbb{P}_W . The resulting density is given by the Girsanov formula $d\mathbb{P}/d\mathbb{P}_W = \exp(-\Phi[\mathbf{x}(t)])$, where Φ is essentially the OM

action minus the diverging \dot{x}^2 term, i.e.

$$\Phi[\mathbf{x}(t)] = \int_0^T \left(\frac{\beta\mu}{4} \mathbf{F}^2 + \frac{\mu}{2} \nabla \cdot \mathbf{F} \right) dt - \frac{\beta}{2} \int_{\mathbf{x}_0}^{\mathbf{x}_T} \mathbf{F} \cdot d\mathbf{X}. \quad (\text{C1})$$

This is a functional on stochastic paths in the TPE [73–75]. The second term in Eq. (C1) is interpreted as an Itô integral. Both integrals in Eq. (C1) are well-defined and finite when evaluated on stochastic paths.

As the Wiener measure \mathbb{P}_W and the Girsanov formula $d\mathbb{P}/d\mathbb{P}_W = \exp(-\Phi[\mathbf{x}(t)])$ provide a mathematically well-defined description of the probability distribution on path space induced by Langevin dynamics, they form a natural starting point for path-sampling algorithms for the TPE. The strategy we follow here is to obtain samples in the target measure \mathbb{P} of the Itô process, by evaluating its density $\exp(-\Phi)$ relative to the Gaussian measure \mathbb{P}_W [69–71]. This is implemented through the pre-conditioned Crank-Nicholson (pCN) Markov Chain Monte Carlo (MCMC) procedure as follows [69–71]. Abstractly, at the n -th iteration a sample $\mathbf{W}^{(n)}$ is drawn from the reference Gaussian measure \mathbb{P}_W , and a Metropolis-Hastings proposal $\tilde{\mathbf{X}}^{(n+1)} = \sqrt{1 - \kappa^2} \mathbf{X}^{(n)} + \kappa \mathbf{W}^{(n)}$ (where $0 < \kappa \leq 1$) is constructed from the current sample transition path $\mathbf{X}^{(n)}$. With probability $p_a = \min\left\{1, \exp(\Phi[\mathbf{X}^{(n)}] - \Phi[\tilde{\mathbf{X}}^{(n+1)}])\right\}$ this proposal is accepted, $\mathbf{X}^{(n+1)} = \tilde{\mathbf{X}}^{(n+1)}$. If the proposal is rejected the current transition path is retained, $\mathbf{X}^{(n+1)} = \mathbf{X}^{(n)}$.

Concretely, to sample from the reference Gaussian measure \mathbb{P}_W , we use its Kosambi-Karhunen-Loève (KKL) expansion [76–78]

$$\mathbf{W}^{(n)}(t) = \mathbf{x}_0 + \bar{\mathbf{v}}t + \sqrt{\frac{2\mu}{\beta}} \sum_{i=1}^{\infty} \mathbf{Z}_i^{(n)} \sqrt{\lambda_i} \phi_i(t) \quad (\text{C2})$$

which starts at \mathbf{x}_0 and ends at \mathbf{x}_T , where $\lambda_i = T^2/\pi^2 i^2$, $\phi_i(t) = \sqrt{2/T} \sin(t/\sqrt{\lambda_i})$, $\bar{\mathbf{v}} = (\mathbf{x}_T - \mathbf{x}_0)/T$ and $\mathbf{Z}_i^{(n)}$ are independent and identically distributed zero-mean unit-variance normal random variables. With the expansion Eq. (C2) generating a sample Gaussian process means drawing a sample of coefficients $\mathbf{Z}_i^{(n)}$. In a key step, which is a new contribution in this Letter, we also expand the stochastic path $\mathbf{X}^{(n)}(t)$ in the same basis as

$$\mathbf{X}^{(n)}(t) = \mathbf{x}_0 + \bar{\mathbf{v}}t + \sqrt{\frac{2\mu}{\beta}} \sum_{i=1}^N \mathbf{Y}_i^{(n)} \sqrt{\lambda_i} \phi_i(t). \quad (\text{C3})$$

where N is a truncation of the expansion to render the algorithm amenable for numerics. Because the Itô process contains a drift term, Eq. (C3) is not a KKL expansion of the Itô process, but a parametrisation of a stochastic path in the TPE in a countably infinite basis and continuous time. The $\mathbf{Y}_i^{(n)}$ are in general not zero-mean unit-variance normal random variables, and their distributions must be obtained through the MCMC procedure. The linearity of the Metropolis-Hastings pCN proposal and the orthogonality of the basis functions $\phi_i(t)$ implies that proposals can be defined directly in coefficient-space $\mathbf{Y}_i^{(n+1)} = \sqrt{1 - \kappa^2} \mathbf{Y}_i^{(n)} + \kappa \mathbf{Z}_i^{(n)}$, with the acceptance probability being determined as before. We also note that the KKL basis allows us to exploit the fast Fourier transform to evaluate Eq. (C3) giving an $O(N \log N)$ efficiency for N degrees of freedom.

To summarize, a step of the pCN algorithm consists of i) sampling from the Wiener measure by drawing a multivariate Gaussian random variable $\mathbf{Z}_i^{(n)}$, ii) calculating the corresponding proposed path coefficients $\mathbf{Y}_i^{(n+1)}$ (which define a proposed transition path via Eq. (C3)), iii) evaluating the Girsanov functional on the proposed path $\Phi[\tilde{\mathbf{X}}^{(n+1)}(t)]$, and iv) accepting the proposed path with probability p_a .

2. Validation of MCMC method

We now compare the results of the MCMC method against a direct Euler-Mayurama integrator on an example system, to verify the validity of the former. As direct methods are generally very inefficient for

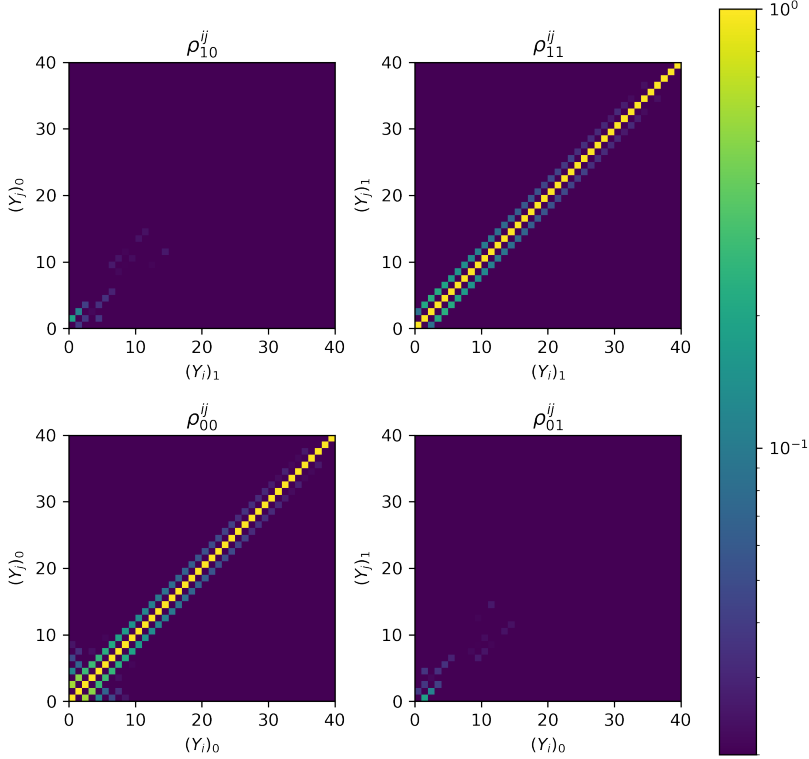


Figure 4. The absolute normalised covariance $\rho_{kl}^{ij} = E^{\mathbb{P}} \{(Y_i)_k (Y_j)_l\} / \sqrt{E^{\mathbb{P}} \{(Y_i)_k^2\} E^{\mathbb{P}} \{(Y_j)_l^2\}}$ of the modes of the sample paths in the KKL basis, found by sampling the system with gradient dynamics using the TMC, at $\theta/\theta_0 = 3.36$, $T/T_0 = 3$ and $N = 200(T/T_0)$.

sampling TPEs, we performed the numerical verification on a simple one-dimensional system, rather than the two-dimensional systems in the main text. Fig. 3 shows a comparison of the results of the MCMC method against a direct simulation of the Langevin equation of an asymmetric double-well potential of the form

$$U(x) = U_0 \left(\left(\frac{x}{L} - 1 \right)^2 - \frac{1}{4} \frac{\Delta U}{U_0} \left(\frac{x}{L} - 2 \right) \right) \left(\frac{x}{L} + 1 \right)^2 \quad (\text{C4})$$

where we have set $\frac{\Delta U}{U_0} = 1/2$. We generated samples of the transition path ensemble with $\tilde{x}(0) = -1$ and $\tilde{x}(T) = 1$. For the Euler-Mayurama method we generated samples by collecting trajectories with end-points within a small interval $\tilde{x}(T) \in [1 - \epsilon, 1 + \epsilon]$ around the right minima, where $\epsilon = 10^{-2}$. As the results of Fig. 3 demonstrates the validity of the MCMC method, we can use the latter to verify the semi-analytical Gaussian mixture approximations.

3. Teleporter MCMC

Here we describe in further detail the *Teleporter MCMC* (TMC) algorithm used in the main text. We start with a discussion of the algorithm in its infinite dimensional form, defined directly on the space of continuous paths, and then proceed to describe a modification of the algorithm adapted to the KKL discretisation.

At each step of the MCMC, with a probability p_{teleport} , we draw an independent proposal step \mathbf{X}' from the mixed Gaussian distribution

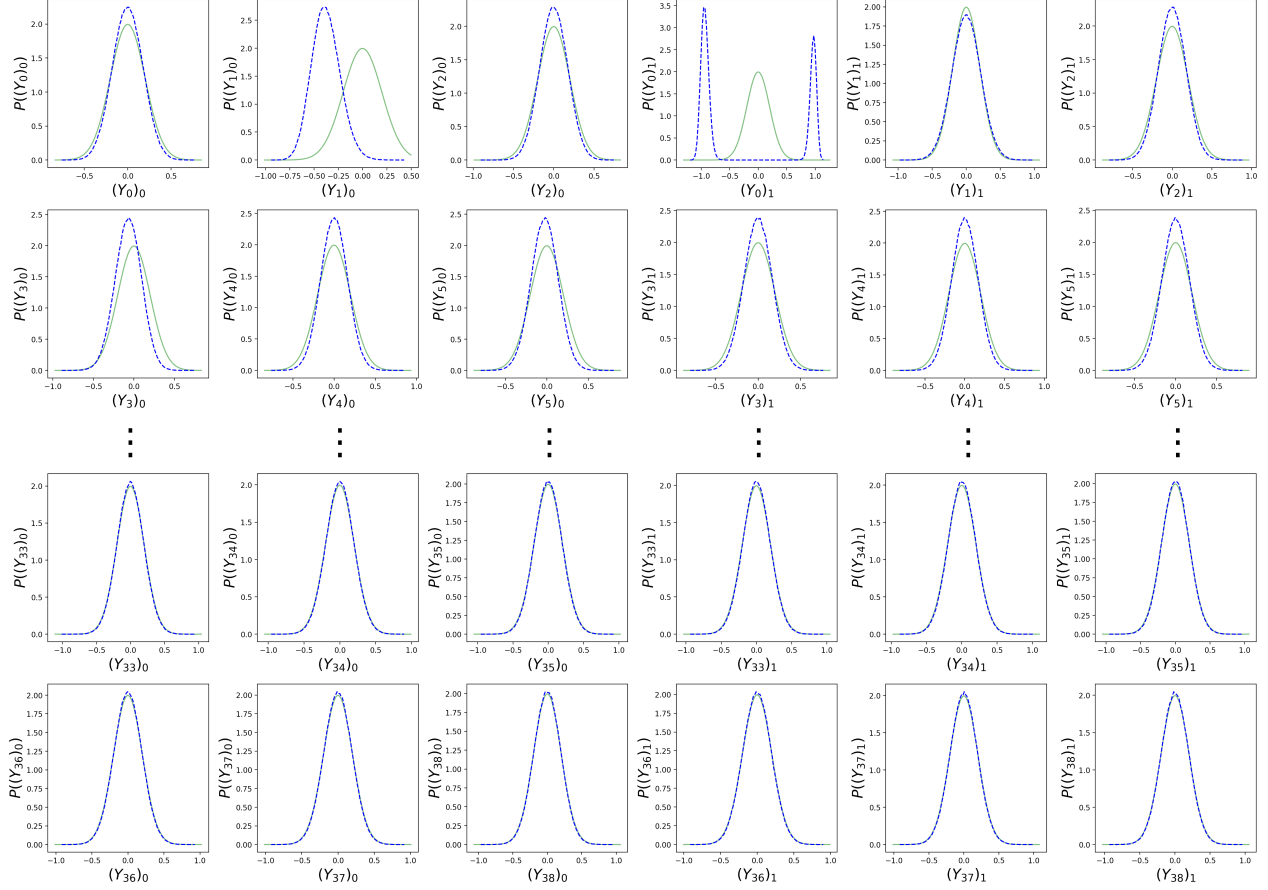


Figure 5. The marginalised distributions of the of the modes of the sample paths (blue) and the Wiener process (green) in the KKL basis, found by sampling the system with gradient dynamics using the TMC, at $\theta/\theta_0 = 3.36$, $T/T_0 = 3$ and $N = 200(T/T_0)$.

$$\bar{\mathbb{P}} = \sum_{\alpha=1}^K w_{\alpha} \mathbb{P}^{[\alpha]} \quad (\text{C5})$$

where the weights w_{α} are parameters that must satisfy $\sum_{\alpha=1}^K w_{\alpha} = 1$, and where $\mathbb{P}^{[\alpha]}$ are Gaussian distributions with precision operators $\mathcal{H}^{[\alpha]}$ and mean $\bar{\mathbf{x}}$ as defined in previous sections. Using the Metropolis-Hastings condition to ensure that the MCMC samples the target measure \mathbb{P} of the Itô process we find that \mathbf{X}' should be accepted with probability

$$a_{\text{TMC}}[\mathbf{X}', \mathbf{X}^{(n)}] = \min \left\{ 1, \exp \left(\Phi[\mathbf{X}^{(n)}] - \Phi[\mathbf{X}'] \right) \frac{\sum_{\alpha} w_{\alpha} \exp(-\Psi^{[\alpha]}[\mathbf{X}^{(n)}])}{\sum_{\alpha} w_{\alpha} \exp(-\Psi^{[\alpha]}[\mathbf{X}'])} \right\} \quad (\text{C6})$$

where $\mathbf{X}^{(n)}$ is current state of the MCMC, and $\Psi^{[\alpha]}$ is the logarithmic density of $\mathbb{P}^{[\alpha]}$ with respect to the Wiener measure $\frac{d\mathbb{P}^{[\alpha]}}{d\mathbb{P}_W} = \exp(-\Psi^{[\alpha]})$ and

$$\Psi^{[\alpha]}[\mathbf{X}] = \Psi_1^{[\alpha]}[\mathbf{X} - \mathbf{x}^{[\alpha]}] + \Psi_2^{[\alpha]}[\mathbf{X}] \quad (\text{C7})$$

$$\Psi_1^{[\alpha]}[\mathbf{X}] = \int_0^T (2\mathbf{X}^T A(t) d\mathbf{X} + \mathbf{X}^T B(t) \mathbf{X} dt) \quad (\text{C8})$$

$$\Psi_2^{[\alpha]}[\mathbf{X}] = \frac{\beta}{2\mu} \int_0^T (2\dot{\mathbf{x}}^{[\alpha]T} d\mathbf{X} - |\dot{\mathbf{x}}^{[\alpha]}|^2 dt) \quad (\text{C9})$$

Thus far, the algorithm has been defined directly on the space of continuous paths, but in numerical applications it is necessary to apply a discretisation procedure. We can approximate $\mathbb{P}^{[\alpha]}$ as a multivariate Gaussian by expanding its precision operator $\mathcal{H}^{[\alpha]}$ in the KKL basis [76–78] of the Wiener process as $(\tilde{H}_{ij}^{[\alpha]})_{kl} = \langle \mathbf{e}_k \phi_i, \mathcal{H}^{[\alpha]} \mathbf{e}_l \phi_j \rangle$, $i, j = 1, \dots, N$, $k, l = 1, \dots, d$, where, \mathbf{e}_k is a constant vector with one non-zero component $(e_k)_l = \delta_{kl}$. Due to our discretisation procedure M can be kept small as the noise dominates over the drift for high-frequency modes, which manifests itself as $\tilde{H}_{ij}^{[\alpha]}$ rapidly converging onto the precision matrix of the Wiener measure, $(H_{ij}^W)_{kl} = \frac{\beta}{4\mu} \delta_{ij} \delta_{kl}$, for high mode numbers i, j . This is demonstrated in Fig. 4 and Fig. 5.

Using the multivariate Gaussian with precision matrix $\tilde{H}^{[\alpha]}$, we construct a grafted Gaussian process $\mathbf{W}^{[\alpha]}(t) = \mathbf{x}^{[\alpha]}(t) + \sqrt{\frac{2\mu}{\beta}} \sum_{i=1}^{\infty} \mathbf{Z}_i^{[\alpha]} \sqrt{\lambda_i} \phi_i(t)$ where $(\mathbf{Z}_1^{[\alpha]}, \dots, \mathbf{Z}_M^{[\alpha]}) \sim \mathcal{N}(0, \tilde{H}^{[\alpha]})$ and $\mathbf{Z}_i^{[\alpha]} \sim \mathcal{N}(0, I_d)$, $i > M$, where I_d is the d -dimensional identity matrix. This defines a Gaussian measure $\tilde{\mathbb{P}}^{[\alpha]}$ on the space of stochastic paths from which we can sample efficiently. Finally, we construct a Gaussian mixture measure as the linear combination

$$\tilde{\mathbb{P}} = \sum_{\alpha=1}^K \tilde{w}_\alpha \tilde{\mathbb{P}}^{[\alpha]} \quad (\text{C10})$$

from which we draw independent samples in the same manner as before. The logarithmic densities of $\tilde{\mathbb{P}}^{[\alpha]}$ with respect to the Wiener measure \mathbb{P}_W are now

$$\tilde{\Psi}^{[\alpha]}[\mathbf{X}] = \sum_{i,j=1}^M \sum_{k,l=1}^d \frac{1}{2} (Y_{ik} - Y_{ik}^{[\alpha]}) \tilde{K}_{ijkl}^{[\alpha]} (Y_{jl} - Y_{jl}^{[\alpha]}) + 2 \sum_{i=1}^M \mathbf{Y}_i^{[\alpha]T} \mathbf{Y}_i + \sum_{i=1}^M \mathbf{Y}_i^{[\alpha]T} \mathbf{Y}_i^{[\alpha]}. \quad (\text{C11})$$

where $\mathbf{X}(t) = \mathbf{x}_0 + \bar{\mathbf{v}}t + \sqrt{\frac{2\mu}{\beta}} \sum_{i=1}^{\infty} \mathbf{Y}_i \sqrt{\lambda_i} \phi_i(t)$, Y_{ik} denotes the k th component of \mathbf{Y}_i , $Y_{ik}^{[\alpha]} = \langle \mathbf{x}^{[\alpha]}, \mathbf{e}_k \phi_i \rangle$, $(\tilde{K}_{ij}^{[\alpha]})_{kl} = \langle \mathbf{e}_k \phi_i, (\mathcal{H}^{[\alpha]} - \mathcal{H}^W) \mathbf{e}_l \phi_j \rangle$, $\tilde{L}_{ik}^{[\alpha]} = \frac{\beta}{2\mu}$ using which the acceptance probabilities are computed as in Eq. (C6).

We now summarise the full algorithm, expressed in the KKL basis:

1. Choose an initial state $\mathbf{Y}^{(0)} \in \mathbb{R}^{N \times d}$.
2. Draw a random number $U^{(n+1)} \sim \text{Unif}([0, 1])$.
 - If $U^{(i+1)} > p_{\text{teleport}}$.
 - (a) Given state $\mathbf{Y}^{(n)}$, the $(n+1)$ -th proposal is

$$\mathbf{Y}'_i = \sqrt{1 - \kappa^2} \mathbf{Y}_i^{(n)} + \kappa \mathbf{Z}_i^{(n)} \quad (\text{C12})$$

where $\mathbf{Z}_i^{(n)} \sim \mathcal{N}(0, I_d)$ and $i = 1, \dots, N$.

- (b) Draw a random number $V^{(n+1)} \sim \text{Unif}([0, 1])$.
 - If $V^{(i+1)} < a[\mathbf{x}(t; \mathbf{Y}'), \mathbf{x}(t; \mathbf{Y}^{(n)})]$ then set $\mathbf{Y}^{(n+1)} = \mathbf{Y}'$.
 - Otherwise set $\mathbf{Y}^{(n+1)} = \mathbf{Y}^{(n)}$.

- If $U^{(i+1)} \leq p_{\text{teleport}}$:

(a) Given state $\mathbf{Y}^{(n)}$, the $(n+1)$ -th proposal is

$$\mathbf{Y}'_i = \tilde{\mathbf{Z}}_i^{(n)} \quad (\text{C13})$$

where $\tilde{\mathbf{Z}}^{(n)}$ is drawn from $\tilde{\mathbb{P}}_N$, and $i = 1, \dots, N$.

- (b) Draw a random number $W^{(n+1)} \sim \text{Unif}([0, 1])$.
- If $W^{(i+1)} < a_{\text{TMC}}[\mathbf{x}(t; \mathbf{Y}'), \mathbf{x}(t; \mathbf{Y}^{(n)})]$ then set $\mathbf{Y}^{(n+1)} = \mathbf{Y}'$.
 - Otherwise set $\mathbf{Y}^{(n+1)} = \mathbf{Y}^{(n)}$.

3. Repeat step 2.

where $\text{Unif}([0, 1])$ is the uniform distribution over the unit interval, $\mathbf{x}(t; \mathbf{Y}) = \mathbf{x}_0 + \bar{\mathbf{v}}t + \sqrt{\frac{2\mu}{\beta}} \sum_{i=1}^N \mathbf{Y}_i \sqrt{\lambda_i} \phi_i(t)$, and $\tilde{\mathbb{P}}_N$ is the truncation of Eq. (C10) to N modes. In the numerical experiments discussed in the main text, we used $\tilde{w}_1 = \tilde{w}_2 = 1/2$ and $M = 10(T/T_0)$.

As mentioned in the main text, an alternate method to the above would be a synthesis of the two sampling approaches in the above algorithm. We could replace the reference Wiener measure \mathbb{P}_W with the mixed Gaussian $\tilde{\mathbb{P}}$, and thus perform the pCN-MCMC with $\tilde{\mathbb{P}}$ as the invariant measure.